Chapter 11

Control and Estimation of a Variable Pitch Wind Turbine for Maximum Power Point Tracking

Ranjan Vepa

Additional information is available at the end of the chapter

http://dx.doi.org/10.5772/62723

Abstract

In this chapter, the design of a nonlinear rotor-side controller is described for a variable pitch wind turbine based on nonlinear, H_2 optimal control theory. The objective is to demonstrate the synthesis and application of a maximum power point tracking (MPPT) algorithm. In the case of a variable pitch wind turbine, the blade collective pitch angle is controlled to ensure that the turbine is not overloaded. In the case of such turbines the blade pitch may be treated as unknown input and the actual pitch angle is estimated in real time from torque measurements. The algorithm uses a non-linear estimation technique and maximizes an estimate of the actual power transferred from the turbine to the generator. It is validated by simulating the wind-turbine's dynamics. It is shown that the MPPT algorithm performs within prescribed error bounds both in the case when no disturbances are present, as it is an indicator of the validity of the algorithm and in cases when significant levels of wind disturbances are present.

Keywords: control system, Kalman filtering, nonlinear estimation, nonlinear filters, simulation, state estimation, induction generators, tracking, tracking filters, wind power generation

1. Introduction

The extraction and regulation of the power from the wind by a wind turbine followed by the capture of this power by a generator has been the subject of several recent research investigations. The use of a doubly fed induction generator (DFIG) is one of most popular options for large-scale electromechanical conversion of wind power to electrical power. The DFIG employs a two-sided controller, a rotor-side controller (RSC) to control the speed of operation and the reactive power, and a grid-side controller (GSC) using a grid-side voltage source converter

which is responsible for regulating the DC link voltage as well as the stator terminal voltage. The rotor-side controller is expected to (i) minimize or regulate the reactive power and hold the stator output voltage frequency constant by a form of current control, (ii) regulate the rotor speed to maintain stable operation, and (iii) alter the speed set point to ensure maximum wind power capture. The role of the grid-side controller is to ensure regulation of the DC voltage bus, and thereby indirectly control the stator terminal voltage. In the case when the generator is feeding an AC-grid, it can be designed to control the power factor. In a typical system, the stator phase voltages and the stator, rotor, and grid phase voltages are assumed to be measured. It is usual to connect the grid-side converter to the grid via chokes to filter the current harmonics. An AC-crowbar is generally included to avoid DC-link over-voltages during grid faults.

It is well known [1] that only a fraction of the power available in the wind is captured by a wind turbine. There is further reduction in the actual power converted to useful power by the generator. The fraction of the power captured by the wind turbine, which is theoretically limited by the so called Betz limit (about 58%), known as the power coefficient is primarily a function of the tip speed ratio, and is usually less than a certain peak value which is about 45% [1]. Maximum energy conversion is possible when the turbine operates at an optimum tip speed ratio which depends on the variation of the power coefficient with respect to the tip speed ratio. The relationship between the power coefficient and the tip speed ratio can be best determined experimentally. In the case of most of the current horizontal axis wind turbines operating at optimum speed, this can be accomplished by indirect control of the rotational speed. The indirect control of the speed is realized by directly controlling the reaction torque of the electric generator [2]. When the principal variables can all be measured, then one could employ one of a large number of maximum power point tracking (MPPT), algorithms have developed. The concept of maximum power point tracking was first introduced in the design of solar panels for spacecraft in the 1970s with the objective of maximizing the power transfer from the photo-voltaic power sources.

In a recent paper [3], the design of a nonlinear rotor-side controller for a wind turbine generator was developed based on nonlinear, H_2 optimal control theory. The objective was to demonstrate the synthesis of a maximum power point tracking (MPPT) algorithm for transferring the maximum power from the turbine to the generator. In the case of a doubly fed induction generator, it was essential that the rotor-side controller and the MPPT algorithm are synthesized concurrently as the nonlinear perturbation dynamics about an operating point is either only just stable or unstable in most real generators. The algorithm uses a non-linear estimation technique and maximizes an estimate of the actual power transferred from the turbine to the generator. It is validated by simulating the wind-turbine's dynamics. In ref. [3], the estimation method was based on the unscented Kalman filter (UKF) and compared with the traditional extended Kalman filter (EKF). The implementation of the algorithm required modelling the real wind velocity profiles from a broadband white noise generator, and by using low order spectrum shaping filters that are derived from approximations of the Kaimal wind velocity spectrum. The simulation was completely executed in the MATLAB environment. The simulation was based on executing the UKF estimator as well as numerically integrating step by step, in parallel, the process model with the feedback controller included in the dynamic

http://dx.doi.org/10.5772/62723

model, about the steady equilibrium solution without linearizing the dynamics. The MPPT algorithm was successfully demonstrated in cases when significant levels of wind disturbances are present. In particular the actual power transferred is compared with maximum available power in the wind, and it is shown in ref. [3] that the maximum power is transferred from the wind to the generator by the turbine.

When applying this algorithm to a real wind turbine, it was found that for purposes of ensuring that the turbine was not overloaded, the collective pitch angle of the turbine's blades could be controlled so as to be able to limit the maximum power captured by the wind turbine. When the pitch of the blades is controllable there are two control inputs to consider. While the blade pitch angle can be used to regulate the capture of the power from the wind by the wind turbine rotor, controlling the generators reaction torque allows for the power to be smoothly converted into electrical energy. For such variable pitch wind turbine, it was found that in order to implement the algorithm developed in ref. [3], it was essential to either measure the blade pitch angle or the torque on the turbine shaft, which is then used to estimate the true wind turbine aerodynamic torque and the blade pitch angle. In the latter case only a model of the closed loop collective pitch angle dynamics is essential. As there were no other benefits of measuring the blade pitch angle, the second option was preferred. The blade pitch angle was then considered as an unknown input to the torque, and it was estimated from the measurements.

In this chapter the modified MPPT algorithm, in the presence of unknown inputs to the aerodynamic torque, is successfully demonstrated both in the case when no disturbances were present, as it is a prerequisite for successful implementation, and in cases when significant levels of wind disturbances are present.

2. The electro-mechanical model of a wind turbine

There have been a number of papers on the subject of modelling of a wind turbine driving an induction generator under turbulent or stochastic wind conditions [4–7]. In this section the electro-mechanical model used in this study which is identical to the model used in ref. [3], is briefly summarized.

2.1. The mechanical model

The mechanical model of the wind turbine is described by,

$$J_{eq} d\omega_m / dt + B_{eq}\omega_m = T_{wt} - T_{mel} \tag{1}$$

where, as defined in ref. [3], ω_m is the mechanical speed of the generator shaft, T_{wt} is the torque extracted by the turbine from the wind, T_{mel} is the mechanical equivalent of the electromagnetic load torque, J_{eq} is the equivalent total inertia of the generator shaft and B_{eq} is the equivalent total friction coefficient. The electromagnetic load torque $T_{mel} = (P/2)T_{el}$ is a linear function of the number of poles P and may be estimated from the electromagnetic reaction torque of the

electric generator per pole pair T_{el}. The torque extracted by the wind turbine T_{wt} is related to the total power absorbed by the turbine from the wind which may respectively be expressed as,

$$T_{wt} = P_w / \omega_m$$

and

$$P_w = \frac{1}{2}\rho\left(\pi R^2\right)C_p\left(\lambda\right)U^3 \tag{2}$$

In the above expression ρ is the density of the air at the hub of the turbine, R is the rotor radius, $C_p(\lambda)$ is a power coefficient which is a function of $\lambda = R\omega_m/U$, the tip speed ratio and U is the wind velocity. Thus, the mean torque may be expressed as,

$$T_{wt} = \rho\left(\pi R^3\right)C_q\left(\lambda\right)U^2/2,$$

$$C_q\left(\lambda\right) = C_p\left(\lambda\right)/\lambda. \tag{3}$$

There are several approximations [8, 9] of $C_p(\lambda)$ in use and a typical approximation in terms of the blade collective pitch angle θ is given by,

$$C_p = 0.22\left(\frac{116}{\lambda_i} - 0.4\times\theta - 5\right)e^{-12.5/\lambda_i}, \tag{4a}$$

$$\frac{1}{\lambda_i} = \frac{1}{\lambda + 0.08\theta} - \frac{0.035}{1+\theta^2} \tag{4b}$$

Typically depending on the approximation used the maximum power coefficient varies over the range, $0.44 \le C_p(\lambda)_{\max} \le 0.492$ and the corresponding tip speed ratio varies over the range, $6.9 \le \lambda_{\max} \le 8.8$.

2.2. The dynamics and control of the pitch angle

The dynamics of variable pitch wind turbine blades plays a key role in the capture and regulation of the power from the wind by the wind turbine rotor. In the case of a horizontal axis wind turbine, there are up to five blades which are assumed to be equi-spaced and to lie with the plane of the rotor disc. The most popular choice for most variable pitch wind turbines

http://dx.doi.org/10.5772/62723

is a three bladed rotor. The dynamics of a variable pitch wind turbine blade can be expressed either in a frame that is fixed in the blade or in a frame that is fixed to the rotor disc. It is convenient to represent the aerodynamic forces in a frame fixed to the blade, while the wind inputs and gusts are more easily represented in a frame fixed to the rotor disc plane. In most practical horizontal wind turbine designs, the rotor disc plane usually aligns itself normal to the wind direction. Thus both frames of reference are used in the dynamical analysis of wind turbines and are transformed from one to the other as and when this is required.

The rotor dynamic model is typically described in terms of non-dimensional quantities so that the general rotor configurations can be analyzed without the need to specify the size. Because of the similarity between the mechanical designs of the rotor for a helicopter, the development of the model closely follows the methodology outlined by Padfield [10] and Fox [11]. The important rotor blade properties of interest are the aerodynamic forces and moments acting on the individual blades, as well as the rotor thrust and torque which are related to the blade forces. Each blade is assumed to be fully controllable in pitch with the root of the blade offset from the rotor axis. The Lock number is an important non-dimensional aerodynamic parameter, and is used to characterize the rotor dynamics parameters. The aerodynamically coupled flap-pitch equations of motion of a single blade are derived in a rotating frame as function of the azimuth angle. To derive the equations of motion of all the blades as a single unit, the coefficients in the equations may be expressed in terms of the so called multi-blade coordinates. This is done by expanding all trigonometric functions such as products of sine and cosine functions as the sums of relevant sine and cosine terms. Thus the fixed frame equations of motion obtained by applying multi-blade coordinate transformations will represent the dynamics of the rotor disc containing N blades. The model of the inflow dynamics is based on the finite state approximation developed by Pitts and Peters [12]. The wind is responsible in generating the primary moment acting on the rotor resulting in a rotor torque, which produces the dominant component of the moment about the rotor shaft axis, which is converted into electrical energy by the generator. This torque can be obtained by integrating the moments of the in-plane aerodynamic pressure distribution acting on the blades about the shaft axis.

Broadly, the approaches to pitch control may be classified into two groups. In a direct pitch controlled system, the controller monitors the wind-turbine's power output at every sampling instant. When the power output exceeds an upper bound, the blade pitch is altered to lower the power generated by the turbine. Increasing the pitch attitude generally reduces the power output. When the maximum power output of the turbine is within the safe operating limits, the pitch angle is reduced to zero.

The second approach to pitch control involves operating the wind turbine with the blades pitched at angle just below the stall angle. The geometry of the blade profile and twist, however are aerodynamically tailored to ensure that when the induced wind speed is high, the angle of attack also increases and the blade begins to stall. The stalling of the lift generated restricts the magnitude of the lift generated and consequently the power generated is also limited. In an actively stall controlled turbine, the pitch of the blade is maintained just below the critical stall angle as long as the power generated by the wind turbine is within the safe operating limits, and increased beyond the critical value when it is desired to stall the generation of lift

on the blade. Thus, when the generator is overloaded, the controller will pitch the blades in the opposite direction from what a pitch controlled machine does, in order to make the blades go into an increased state of stall.

The approximation to $C_p(\lambda)$ given by equations (4a) and (4b) are only valid or small increments in the blade pitch angle, and do not include the influence of blade stall. For this reason, in this work, we consider only a pitch controlled wind-turbine. To model the blade dynamics, it is first required to model the open loop dynamics. Once the open loop pitch dynamics is obtained, it is assumed that an appropriate feedback law is designed. Thus, what is important is the closed loop dynamics of the pitch angle which is represented by a reduced, first order model of the form,

$$\tau \frac{\partial \theta(t)}{\partial t} + \theta(t) = \theta_{demand} \tag{5}$$

Thus the discrete dynamics of the pitch angle may be expressed as,

$$\theta_{k+1} - \theta_k = \frac{\Delta t}{\tau}\left(\theta_{demand} - \theta_k\right) \tag{6}$$

The model may be used to design control laws for both active pitch controlled and active stall controlled wind-turbines. The demanded blade pitch angle θ_{demand}, is set by the unconstrained minimization of the square of the error between the desired output power and the actual power generated by the wind turbine rotor.

To design an active stall controller, the first step is to model the section lift and drag coefficients of the blade when the section angle of attack exceeds the stall angle. Modes of both the section lift and drag coefficients of the blade when the section angle of attack exceeds the stall angle have been presented by Tangler and Kocurek [13] and by Tangler and Ostowari [14] based on a model developed by Viterna and Corrigan [15]. These are then substituted into the expression for the power coefficient developed on the basis of the blade element momentum theory (see for example Vepa [16], Section 4.4.1). Once the expression for the power coefficient is found, the commanded blade angle is found by requiring the error between the actual power generated, estimated from the power coefficient, and the maximum power is a minimum.

2.3. The nonlinear dynamic electro-mechanical model

The basic equations of the dynamics of the doubly fed induction machine can be established as done in ref. [3], by considering the equivalent circuit of a single stator phase and a single rotor phase and the mutual coupling between the stator and rotor phases. The voltage vector consisting of the voltages applied to each stator and rotor phases is related to the voltage drops across the resistances of these phases and the rate of change of the fluxes linking the stator and rotor phases. The fluxes in turn are related to the current vector via a matrix of inductances

http://dx.doi.org/10.5772/62723

which are not constant but period functions of time with the period equal to the rotor's electrical speed, $\omega_e = P\omega_m$, which is the product of the number of pole pairs, P and the rotor's mechanical speed, ω_m. When all of the stator and rotor quantities are transformed to a stationary frame (the d–q frame) using the standard Park-Blondel transformation, in terms of the stator's and rotor's voltage oscillation frequencies $\omega_s$and ω_r respectively, the dynamic equations reduce to a set of four with constant coefficients as derived in ref. [3]. Moreover $\omega_r = \omega_s - \omega_e$ can be found by measuring ω_s and ω_e, and is also the slip frequency. (The ratio $s = \omega_r/\omega_s$ is the slip.)

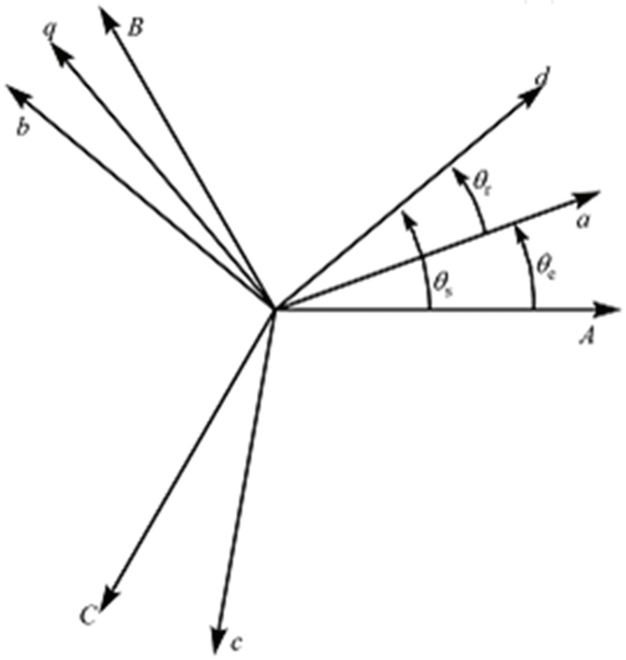

Figure 1. Relationships between the d–q frame and the stator and rotor phases.

The phase angles relating the directions of the d–q frame and the phase angles of the first of the three stator phases, A, B, and C, θ_s and the first of the three rotor phases, a, b and c, θ_r satisfy the relation $\theta_r = \theta_s - \theta_e$ where θ_e is the rotor's electrical angle as illustrated in **Figure 1**. In modeling the stator of DFIG, the generator convention that positive direction of electromagnetic torque is in the direction opposing to the direction of rotation is used, while in modeling the rotor of DFIG the motor convention is used. The dynamic equivalent circuit of generator in synchronous rotating reference frame, the d–q frame, is used to set up the model equations.

The dynamical equations of the DFIG relating the voltages in the stator and rotor and in the d–q frame to the currents, fluxes and the flux rates are,

$$v_{ds} = R_s i_{ds} + \frac{d\varphi_{ds}}{dt} - \omega_s \varphi_{qs} \ , v_{qs} = R_s i_{qs} + \frac{d\varphi_{qs}}{dt} + \omega_s \varphi_{ds} \ , \tag{7a}$$

$$v_{dr} = R_r i_{dr} + \frac{d\varphi_{dr}}{dt} - \omega_r \varphi_{qr} \ , v_{qr} = R_r i_{qr} + \frac{d\varphi_{qr}}{dt} + \omega_r \varphi_{dr} \tag{7b}$$

The stator fluxes are related to the stator and rotor currents in the *d–q* frame as,

$$\varphi_{ds} = L_s i_{ds} + L_m i_{dr} \ , \varphi_{qs} = L_s i_{qs} + L_m i_{qr} \tag{8a}$$

The rotor fluxes are related to the stator and rotor currents in the *d–q* frame as,

$$\varphi_{dr} = L_r i_{dr} + L_m i_{ds} \ , \varphi_{qr} = L_r i_{qr} + L_m i_{qs} \tag{8b}$$

In the above equations, as defined in ref. [3], L_s,L_r,R_s, and R_r, are respectively the self-inductances and resistances of the stator and rotor windings. The quantity L_m is the mutual inductance between a stator and a rotor phase when they are fully aligned with each other.

At the stator terminals, the active and reactive components of the power are given by,

$$P_s = v_{ds} i_{ds} + v_{qs} i_{qs} \ , Q_s = v_{qs} i_{ds} - v_{ds} i_{qs} \tag{9a}$$

At the rotor terminals, the active and reactive components of the power are given by,

$$P_r = v_{dr} i_{dr} + v_{qr} i_{qr} \ , Q_r = v_{qr} i_{dr} - v_{dr} i_{qr} \tag{9b}$$

The active and reactive powers exchanged by the generator and the grid are respectively the sum of the active and reactive components of the power at the stator and rotor. The electromagnetic reaction torque may be expressed as,

$$T_{el} = \left(\varphi_{ds} i_{qs} - \varphi_{qs} i_{ds} \right) \tag{10}$$

Assuming that the stator flux is stationary in the *d–q* frame and neglecting the stator's resistive voltage drop v_{ds} = 0. Hence the *q* – component of the stator voltage may be expressed as, $v_s = v_{qs}$. Assuming further that a grid-side controller is in place and choosing a stator-flux oriented reference frame, the *d*-axis is aligned with the stator flux linkage vector, φ_s; thus $\varphi_{ds} = \varphi_s$ and $\varphi_{qs} = 0$. From equations (8a) and (7a), i_{ms} is defined by,

$$\varphi_s = L_s i_{ds} + L_m i_{dr} = \frac{1}{\omega_s} \left(v_{qs} - R_s i_{qs} \right) \equiv L_m i_{ms} \tag{11a}$$

http://dx.doi.org/10.5772/62723

Thus, from equations (8a),

$$L_s i_{ds} = L_m \left(i_{ms} - i_{dr} \right), L_s i_{qs} = -L_m i_{qr} \tag{11b}$$

Eliminating i_{ds} and i_{qs} from equations (7b) and (8b) it can be shown that, the rotor flux components are,

$$\varphi_{dr} = L_r \left(\frac{L_s L_r - L_m^2}{L_s L_r} \right) i_{dr} + \frac{L_m^2}{L_s} i_{ms} \ , \ \varphi_{qr} = L_r \left(\frac{L_s L_r - L_m^2}{L_s L_r} \right) i_{qr} \tag{11c}$$

The electromagnetic reaction torque given by equation (10) and the reactive power at the stator terminal given by the second of equations (9a) may also be expressed in terms of i_{ms} as,

$$T_{el} = \varphi_s i_{qs} = -L_m^2 i_{ms} i_{qr} / L_s \ , \tag{12a}$$

$$Q_s = v_{qs} i_{ds} - v_{ds} i_{qs} = \omega_s \varphi_s i_{ds} = \omega_s L_m^2 i_{ms} \left(i_{ms} - i_{dr} \right) / L_s \tag{12b}$$

Defining the mutual inductance coupling coefficient σ as,

$$\sigma = \left(L_s L_r - L_m^2 \right) / L_s L_r \tag{13}$$

and using equations (11c) with $v_{ds} = 0$ and $v_s = v_{qs}$ the rotor voltage equations given by the equations (7b) are expressed as,

$$v_{dr} = R_r i_{dr} + \sigma L_r \frac{di_{dr}}{dt} - \sigma s \omega_s L_r i_{qr} \tag{14a}$$

$$v_{qr} - s \frac{L_m}{L_s} v_s = \left(R_r + s \frac{L_m^2}{L_s^2} R_s \right) i_{qr} + \sigma L_r \frac{di_{qr}}{dt} + \sigma s \omega_s L_r i_{dr} \tag{14b}$$

The total reactive power is $Q = Q_r + Q_s$ where Q_s is given by equations (11a) and (12b), with $v_{ds} = 0$ and $v_s = v_{qs}$. Thus the total reactive power is,

$$Q = v_{qr} i_{dr} - v_{dr} i_{qr} + \omega_s \frac{L_m^2}{L_s} \times \left(\frac{v_s}{\omega_s L_m} + \frac{R_s}{\omega_s L_m} i_{qr} \right) \left(\frac{v_s}{\omega_s L_m} + \frac{R_s}{\omega_s L_m} i_{qr} - i_{dr} \right) \tag{15}$$

The definitions of the resistances and inductances and their typical values assumed in this chapter are listed in **Table 1**.

P	**Number of poles**	**6**
R_s	Stator resistance	0.95 Ω
L_s	Stator inductance	94 mH
L_m	Magnetizing inductance	82 mH
R_r	Rotor resistance	1.8 Ω
L_r	Rotor inductance	88 mH
V_a	Stator phase voltage	380 V
	Grid frequency	50 Hz
	Nominal mechanical rotor speed	100 rads/sec
	Rated maximum power	100 kW

Table 1. Definitions and typical values assumed for the generator's parameters.

In steady state, assuming that,

$$v_{dr} = v_{dr}^0,\ v_{qr} = v_{qr}^0,\ i_{dr} = i_{dr}^0,\ i_{qr} = i_{qr}^0,\ s = s^0, \tag{16}$$

where the superscript '0' refers to the steady-state condition, and subtracting the steady-state components from (14a) and (14b), the electro-mechanical perturbation equations are obtained. The perturbation states, inputs and variables are defined as:

$$\begin{aligned} \Delta v_{dr} = v_{dr} - v_{dr}^0,\ \Delta v_{qr} = v_{qr} - v_{qr}^0,\ \Delta i_{dr} = i_{dr} - i_{dr}^0,\ \Delta i_{qr} = i_{qr} - i_{qr}^0, \\ \Delta s = s - s^0 = -\frac{\Delta \omega_e}{\omega_s},\ \Delta \omega_e = \omega_e - \omega_e^0. \end{aligned} \tag{17}$$

Given that $T_{wt} = T_{wt}^0$ in steady-state and that $\Delta T_{wt} = T_{wt} - T_{wt}^0$, $\Delta \omega_e$ satisfies the equation,

$$J_{eq}\frac{d\Delta\omega_e}{dt} + B_{eq}\Delta\omega_e = \frac{P}{2}\left(\Delta T_{wt} - \frac{P}{2}T_{el} + \frac{P}{2}T_{el}^0\right) \tag{18}$$

Using equation (11a) and introducing the steady state and perturbation variables, the expression for the electromagnetic torque is,

$$T_{el} = T_{el}^0 - \frac{L_m^2}{L_s}\left(\frac{v_s}{\omega_s L_m} + \frac{R_s}{\omega_s L_s}\left(2i_{qr}^0 + \Delta i_{qr}\right)\right)\Delta i_{qr} \tag{19}$$

The wind turbine perturbation torque $\Delta T_{wt}(U,\ \omega_e) = \left(T_{wt}(U,\ \omega_e) - T_{wt}\left(U_0,\ \omega_e^0\right)\right)$, is a function of two variables, the wind speed U, and the rotor speed ω_e. Given that the wind speed, $U = U_0 + \Delta u_f$ is the sum of a mean component, U_0 and a fluctuating component, Δu_f, the wind turbine perturbation torque can be considered to be made of two components,

$$\Delta T_{wt}\left(U,\omega_e\right) = \left(T_{wt}\left(U,\omega_e\right) - T_{wt}\left(U_0,\omega_e\right)\right) +$$

$$\left(T_{wt}\left(U_0,\omega_e\right) - T_{wt}^0\left(U_0,\omega_e^0\right)\right) = \Delta T_{wt}\big|_{\omega_e} + \Delta T_{wt}\big|_{U=U_0} \tag{20}$$

where the first component is evaluated at the current rotor speed, ω_e and the second at the mean wind speed, U_0. Hence, without making any assumptions that the perturbations are small, the equation for mechanical motion, equation (18), may be expressed as,

$$J_{eq}\frac{d\Delta\omega_e}{dt} = \left(\frac{P}{2}\frac{\Delta T_{wt}}{\Delta\omega_e}\bigg|_{U=U_0} - B_{eq}\right)\Delta\omega_e +$$

$$\frac{P^2}{4}\frac{L_m^2}{L_s}\left(\frac{v_s}{\omega_s L_m} + \frac{R_s}{\omega_s L_s}\left(2i_{qr}^0 + \Delta i_{qr}\right)\right)\Delta i_{qr} + \Delta T_{wt}\big|_{\omega_e} \tag{21}$$

while the electrical machine perturbation equations are,

$$\sigma L_r\frac{d\Delta i_{dr}}{dt} = -\sigma L_r i_{qr}\Delta\omega_e - R_r\Delta i_{dr} + \sigma s^0\omega_s L_r\Delta i_{qr} + \Delta v_{dr} \tag{22a}$$

$$\begin{aligned}\sigma L_r\frac{d\Delta i_{qr}}{dt} = &+\left(\sigma L_r i_{dr} + \frac{L_m^2}{\omega_s L_s^2}R_s i_{qr}\right)\Delta\omega_e - \sigma s^0\omega_s L_r\Delta i_{dr}\\ &-\left(R_r + s^0\frac{L_m^2}{L_s^2}R_s\right)\Delta i_{qr} + \Delta v_{qr}\end{aligned} \tag{22b}$$

Assuming that

$$\Delta v_{dr} = \Delta v_{dr}^{+} + \sigma L_r i_{qr} \Delta\omega_e - R_r^{+} \Delta i_{dr} + \sigma s^0 \omega_s L_r \Delta i_{qr} \ , \tag{23}$$

equations (21) and (22) may be partially decoupled, and (22a) may be treated independently. Thus the complete non-linear equations for the perturbation states used for the design of the nonlinear rotor-side controller may be expressed in state space form as,

$$\frac{d}{dt}\begin{bmatrix} \Delta\omega_e \\ \Delta i_{qr} \end{bmatrix} = \mathbf{A}\begin{bmatrix} \Delta\omega_e \\ \Delta i_{qr} \end{bmatrix} + \frac{1}{\sigma L_r}\begin{bmatrix} 0 \\ 1 \end{bmatrix}\Delta v_{qr} + \begin{bmatrix} 1 \\ 0 \end{bmatrix}\alpha_u \tag{24a}$$

where

$$\alpha_u = \left(\Delta T_{wt} / \Delta u_f\big|_{\omega_e} / J_{eq}\right)\Delta u_f \tag{24b}$$

is the disturbing angular acceleration on the rotor due to wind speed fluctuating component and **A** is a matrix of functional coefficients.

R	**Wind turbine blade disc radius**	**6 m**
	Number of blades	3
U_0	Nominal wind speed	10 m/s
P_n	Wind power at nominal wind speed	~10 kW
	Gearbox ratio	10
J_{eq}	Rotor inertia	40 kgm^2
B_{eq}	Viscous friction coefficient	0.07 Nms/rad
	Cut-in wind speed (m/s)	3.5 m/s

Table 2. Definitions and typical values of the wind turbine parameters.

The modeling of the turbulent wind component and the control of wind turbine is based entirely on [3] and will not be repeated here. The complete characteristics of the wind turbine are summarized in **Table 2**.

3. The measurements and nonlinear state estimation

The dynamic model of the wind turbine that must be employed for purposes of state estimation is not only not linear but also involves the estimation of large dynamic signals. The Kalman filter which was formulated in the 1960s is primarily applicable to linear systems. To overcome the limitations imposed by the requirement of linearity, it was subsequently, empirically,

http://dx.doi.org/10.5772/62723

extended and applied to nonlinear systems. A number of approaches such as the extended Kalman filter (EKF) have been proposed in the literature to extend the application of the traditional Kalman filter for nonlinear state estimation. However, the stability of these extended formulations is not guaranteed unlike the linear Kalman filter. Thus the EKF may diverge if the consecutive linearizations are not a good approximation of the linear model over the entire uncertainty domain. Nonetheless the EKF provides a simple and practical approach to dealing with essential non-linear dynamics.

The UKF has been proposed by Julier, Uhlmann, and Durrant-Whyte [17], and used in ref. [3]. It can overcome the limitations of applying the Kalman filter to nonlinear systems. The UKF based on the unscented transformation of the statistics of a random variable. It provides a method of calculating the mean and covariance of a random variable undergoing a non-linear transformation $\mathbf{y} = \mathbf{f}(\mathbf{w})$. In the main, the method is used to construct a set of *sigma vectors* and propagate them through the non-linear transformation. The mean and covariance of the transformed vector are approximated as a weighted sum of the transformed *sigma vectors* and their covariance matrices. The details may be found in the paper by Julier and Uhlmann [18].

As in ref. [3], given a general discrete nonlinear dynamic system in the form,

$$\mathbf{x}_{k+1} = \mathbf{f}_k\left(\mathbf{x}_k, \mathbf{u}_k^{ui}, \mathbf{u}_k\right) + \mathbf{w}_k,\ \mathbf{z}_k = \mathbf{h}_k\left(\mathbf{x}_k, \mathbf{u}_k\right) + \mathbf{H}_k\mathbf{u}_k^{ui} + \mathbf{v}_k \tag{25}$$

where $\mathbf{x}_k \in R^n$ is the state vector, $\mathbf{u}_k^{ui} \in R^{uk}$ is the unknown input vector, $\mathbf{u} \in R^r$ is the known input vector, $\mathbf{z}_k \in R^m$ is the output vector at time k. $\mathbf{w}_k$ and $\mathbf{v}_k$ are, respectively, the disturbance or process noise and sensor noise vectors, which are assumed to Gaussian white noise with zero mean and are also assumed to be independent of each other. We have tacitly assumed that the unknown input is related to the measurements linearly. Furthermore, $\mathbf{Q}_k$ and $\mathbf{R}_k$ are assumed to be the covariance matrices of the process noise sequence, $\mathbf{w}_k$ and the measurement noise sequence, $\mathbf{v}_k$ respectively. The joint unscented transformation of the states and unknown inputs by the nonlinear function $\mathbf{f}_k\left(\mathbf{x}_k, \mathbf{u}_k^{ui}, \mathbf{u}_k\right)$ is denoted as, $\mathbf{f}_k^{UT} = \mathbf{f}_k^{UT}\left(\mathbf{x}_k, \mathbf{u}_k^{ui}, \mathbf{u}_k\right)$, the unscented transformation of the states by the nonlinear function $\mathbf{h}_k(\mathbf{x}_k, \mathbf{u}_k)$ is denoted as $\mathbf{h}_k^{UT} = \mathbf{h}_k^{UT}(\mathbf{x}_k, \mathbf{u}_k)$ while the transformed covariance matrices and cross-covariance are respectively denoted as, $\mathbf{P}_k^{ff} = \mathbf{P}_k^{ff}\left(\hat{\mathbf{x}}_k, \hat{\mathbf{u}}_k^{ui}, \mathbf{u}_k\right)$, $\mathbf{P}_k^{hh-} = \mathbf{P}_k^{hh}\left(\hat{\mathbf{x}}_k^-, \mathbf{u}_k\right)$ and $\mathbf{P}_k^{xh-} = \mathbf{P}_k^{xh-}\left(\hat{\mathbf{x}}_k^-, \hat{\mathbf{u}}_k^{ui}, \mathbf{u}_k\right)$. In the above unscented transformations $\mathbf{u}_k$ is a deterministic variable while $\mathbf{u}_k^{ui}$ is a stochastic variable which is dealt with by augmenting the state vector $\mathbf{x}_k$ to $\left[\mathbf{x}_k^T \quad \mathbf{u}_k^{ui\,T}\right]^T$ for obtaining $\mathbf{f}_k^{UT}$. We have chosen to use the scaled unscented transformation proposed by Julier [19], as this transformation gives one the added flexibility of scaling the sigma points to ensure that the covariance matrices are always positive definite. The unknown input UKF estimator can then be expressed in a compact form based on the original derivation for the linear case by Pan, Su, Wang, and Chu [20]. The state time-update equation, the propagated covariance, the Kalman gain, the state estimate, and the updated covariance are respectively given by,

$$\hat{\mathbf{x}}_k^- = \mathbf{f}_{k-1}^{UT}\left(\hat{\mathbf{x}}_{k-1}, \hat{\mathbf{u}}_{k-1}^{ui}, \mathbf{u}_{k-1}\right) \tag{26a}$$

$$\hat{\mathbf{P}}_k^{x-} = \mathbf{P}_{k-1}^{ff} + \mathbf{Q}_{k-1} \tag{26b}$$

$$\hat{\mathbf{P}}_k^{zz} = \left(\hat{\mathbf{P}}_k^{hh-} + \mathbf{R}_k\right), \mathbf{K}_k = \hat{\mathbf{P}}_k^{xh-}\left(\hat{\mathbf{P}}_k^{zz}\right)^{-1} \tag{26c}$$

$$\hat{\mathbf{P}}_k^{uu} = \left(\mathbf{H}_k^T\left(\hat{\mathbf{P}}_k^{zz}\right)^{-1}\mathbf{H}_k\right)^{-1}, \hat{\mathbf{P}}_k^{xu} = -\mathbf{K}_k\mathbf{H}_k\hat{\mathbf{P}}_k^{uu} \tag{26d}$$

$$\mathbf{M}_k = \hat{\mathbf{P}}_k^{uu}\mathbf{H}_k^T\left(\hat{\mathbf{P}}_k^{zz}\right)^{-1}, \hat{\mathbf{u}}_k^{ui} = \mathbf{M}_k\left[\mathbf{z}_k - \mathbf{h}_k^{UT}\left(\hat{\mathbf{x}}_k^-\right)\right] \tag{26e}$$

$$\hat{\mathbf{x}}_k = \hat{\mathbf{x}}_k^- + \mathbf{K}_k\left[\mathbf{z}_k - \mathbf{h}_k^{UT}\left(\hat{\mathbf{x}}_k^-\right) - \mathbf{H}_k\hat{\mathbf{u}}_k^{ui}\right], \tag{26f}$$

$$\hat{\mathbf{P}}_k^{x} = \hat{\mathbf{P}}_k^{x-} - \mathbf{K}_k\left(\hat{\mathbf{P}}_k^{zz} - \mathbf{H}_k\hat{\mathbf{P}}_k^{uu}\mathbf{H}_k^T\right)\mathbf{K}_k^T, \tag{26g}$$

$$\hat{\mathbf{P}}_k = \begin{bmatrix} \hat{\mathbf{P}}_k^{x} & \hat{\mathbf{P}}_k^{xu} \\ \left(\hat{\mathbf{P}}_k^{xu}\right)^T & \hat{\mathbf{P}}_k^{uu} \end{bmatrix} \tag{26h}$$

It is possible to estimate the unknown inputs only when the matrix product $\mathbf{H}_k^T\hat{\mathbf{P}}_k^{zz}\mathbf{H}_k$ is invertible. Equations (26a)–(26h), which are referred to as unscented Kalman filter equations with unknown inputs, are used to estimate all the states of the system when only a limited combination of states are measured. Equations (26) are in the same form as the traditional unscented Kalman filter in the absence of the unknown inputs and the traditional extended Kalman filter. Thus, higher order non-linear models capturing significant aspects of the dynamics may be employed to ensure that the Kalman filter algorithm can be implemented to effectively estimate the states in practice.

4. The MPPT outer loop controller

Several algorithms for achieving maximum power tracking and control have been proposed for a number of power systems [21, 22]. There have been a number of MPPT controllers proposed recently for wind turbines based on maximizing the net power captured by the generator [23–26]. A recent book on the topic has covered the optimal control based strategies

http://dx.doi.org/10.5772/62723

quite extensively [27]. There have also been a few methods based on some form of optimal estimation of the wind speed [28]. A nonlinear controller based MPPT method has also been applied to wind turbines [29]. Several of the optimal control strategies may be efficiently implemented for a wind turbine provided that highly reliable non-linear estimation algorithms are used to estimate the states of the wind turbine in operation. In this section, one such approach is briefly outlined and implemented as in ref. [3]. The system now includes the independently controlled variable pitch blades while in ref. [3], only a turbine with fixed blades was considered.

It is assumed that the induction machine is controlled in a manner so as to ensure variable-speed operation over a wide range input conditions, so it is possible to exercise direct control of the system's tip speed ratio. The wind power captured by the wind-turbine is estimated from the state estimates by the equation, $\hat{P}_w = \hat{T}_{wt}\hat{\omega}_m$ where $\hat{T}_{wt}$ is an estimate of the turbine torque and $\hat{\omega}_m$ is an estimate of the mechanical speed. The wind turbine torque may be estimated from the mechanical equation of the shaft rotation by using (1) to develop the equation for the electrical speed ω_e, to give T_{wt}. However, since the pitch angle is not generally known, the wind turbine torque is estimated at the current estimate of the pitch angle and compared with either the measurement of the wind turbine torque or an estimate of the measurement. This process facilitates the update of the estimate of the pitch angle in the first instance. Once the blade pitch angle is updated, the wind turbine torque is estimated at the updated value of the blade pitch angle. With the updated estimate of the wind turbine torque the algorithm for estimating the rotor frequency for maximum power is essentially identical to the method in ref. [3] and briefly summarized in the next paragraph.

The wind turbine torque T_{wt} is a weighted linear combination of T_{el}, $d\omega_e/dt$, and ω_e. When $\hat{P}_w$ is maximum,

$$\frac{d}{d\hat{\omega}_m}\hat{P}_w \equiv \hat{P}_w' = \hat{\omega}_m\left(\frac{d\hat{T}_{wt}}{d\hat{\omega}_m} + \frac{\hat{T}_{wt}}{\hat{\omega}_m}\right) = 0 \tag{27a}$$

The condition for maximum power capture is,

$$\hat{T}_{wt}/\hat{\omega}_m = -d\hat{T}_{wt}/d\hat{\omega}_m \tag{27b}$$

Thus the instantaneous torque speed ratio or the *instantaneous impedance* is equal to the negative of the incremental torque to incremental speed ratio or the *incremental impedance*. This is frequency dependent and is determined when the wind power input is a maximum. It follows that in the nonlinear perturbation equations,

$$\left.\frac{\Delta T_{wt}}{\Delta\omega_e}\right|_{U=U_0} = -\frac{T_{wt}}{\omega_e} \tag{28}$$

In evaluating $\Delta T_{wt} / \Delta u_f \mid_{\omega_e}$, the wind turbine torque perturbation due to a change in the wind speed, the power coefficient, $C_p(\lambda)$ is assumed to be a maximum.

To determine the rotor frequency at which maximum power is extracted from the wind by the turbine, the rotor frequency is assigned an initial value $\omega_p^0 = \omega_{r0}$ and updated at regular time intervals. The update is filtered, driven by an estimate obtained by using the Newton-Raphson formula at each time step *k*, and given by,

$$\omega_p^{k+1} = \omega_p^k + \Delta_k,\ \Delta_{k+1} = \Delta_k + \left(u_k - \Delta_k\right) dt / \tau_{fu} \tag{29a}$$

$$u_k = K_\omega \frac{\hat{P}'_{k-1}\left(\omega_p^{k-1} - \omega_p^{k-2}\right)}{\left(\hat{P}'_{k-1} - \hat{P}'_{k-2}\right)},\ \hat{P}'_k = \hat{\omega}_m^k \frac{d\hat{T}_{wt}^k}{d\hat{\omega}_m^k} + \hat{T}_{wt}^k \tag{29b}$$

The frequency ω_p^k is the estimated rotor frequency at the maximum power point. The optimum time constant $\tau_{fu} \approx 0.04$ and the update gain, $K_\omega \approx 0.27$ were empirically determined after several simulation runs. The turbine torque and its derivative with respect to the estimated mechanical rotor speed $\hat{\omega}_m$ must be evaluated accurately in order to ensure that the turbine operates at the peak power. The turbine torque peaks at a speed slightly less than the speed at which the turbine power is a peak. The full control law for maximum power point tracking takes the form,

$$\omega_r = \omega_p^k \tag{30}$$

where ω_p^k is given by (29a).

5. Typical simulation-based results

To make the comparisons easy and to draw meaningful conclusions, the same example as the one considered in ref. [3] is also considered here with the exception that, in the case considered here, the blade pitch angle was assumed to be independently controlled. The initial equilibrium conditions were deliberately chosen so the nonlinear perturbation dynamics of the turbo-generator about the initial operating point were not stable. So the initial feedback controller was obtained by adopting the LQR-based methodology of Vepa [3] and using a model evaluated at the initial perturbation. Measurements of the rotor speed and the rotor *d–q* currents were generated by adding a random error with zero mean and a specified variance to the simulated outputs. All the perturbation states were estimated using both the UKF and the traditional EKF methodologies. **Figure 2** illustrates the simulated electrical speed of the generator, which is thrice the mechanical speed, for a time step, $dt = 0.001$ s and compared with

http://dx.doi.org/10.5772/62723

the UKF and EKF estimates over a time frame of 20,000 time steps or 20 seconds in real time. The maximum error between the curves is less than 0.2%.

Figure 3 compares the electrical speed error in the measurement, with estimates of it obtained by using the UKF and the EKF. To make the comparison we have zoomed-in over a time frame of the first 50 time steps. Quite clearly the UKF estimate converges rapidly to the measurement while the EKF estimate fluctuates in the vicinity of the measurement. From the comparisons shown in **Figure 3**, the superiority of the UKF over the EKF can be deduced. For purposes of maintaining clarity, all the other results corresponding to the EKF estimates are not shown in the figures.

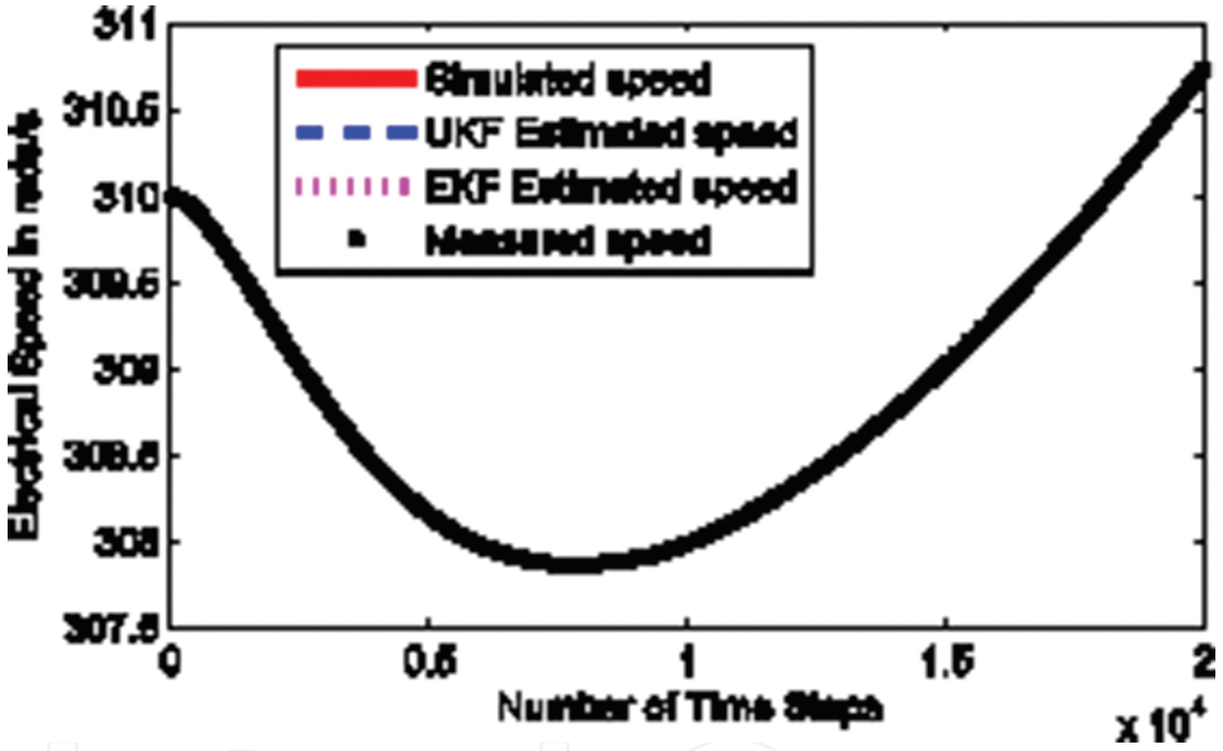

Figure 2. Simulated electrical speed (in rads/s) response of the DFIG generator compared with the measurement, the UKF and the EKF estimates.

Using this algorithm repeatedly has accentuated the need for making accurate electrical speed rate measurements and estimates. The electrical speed rate estimation was done using measurements of the electrical speed rate. From the previously estimated electrical speed and independently processing the measured electrical speed rate in another first order mixing filter, the estimates of the electrical speed are continuously updated. This approach provides precise estimates of the speed rate and facilitates the accurate estimation of the torque absorbed by the turbine from the wind. **Figure 4** shows the corresponding power transferred from the wind to the generator over the first 20,000 time steps and compared with maximum available wind power at that particular maximum magnitude of the wind speed and zero blade pitch angle.

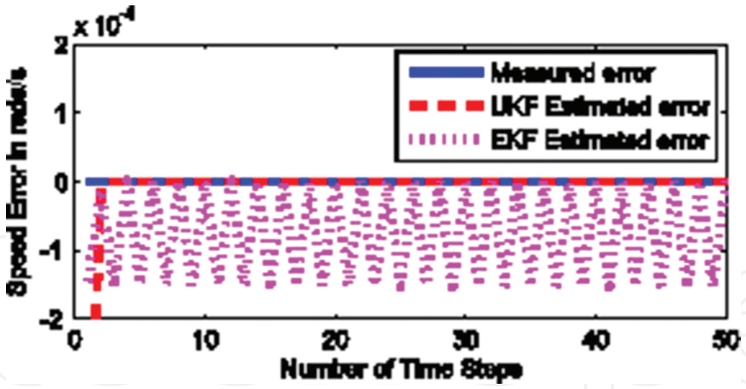

Figure 3. Comparison of the measured and UKF and EKF estimated electrical speed (in rads/s) errors corresponding to **Figure 2**.

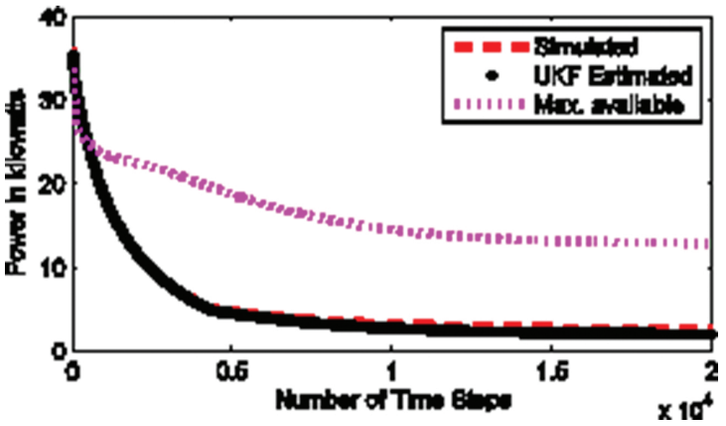

Figure 4. Wind power transferred to the generator over the first 20,000 time steps and compared with maximum available wind power.

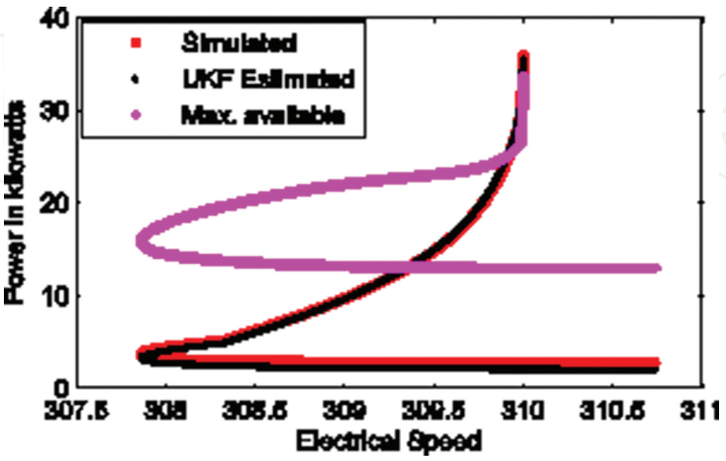

Figure 5. Turbine power characteristic over the operating speeds in rad/s.

http://dx.doi.org/10.5772/62723

Figure 5 illustrates the power speed characteristic corresponding to **Figure 4**. From **Figures 4** and **5**, it may be observed that the power transferred by the turbine from the wind to the generator tracks the maximum available wind power. **Figures 6** and **7** illustrate the corresponding torque on the generator and the torque-electrical speed characteristic. Also shown on these figures is the torque corresponding to the maximum available power.

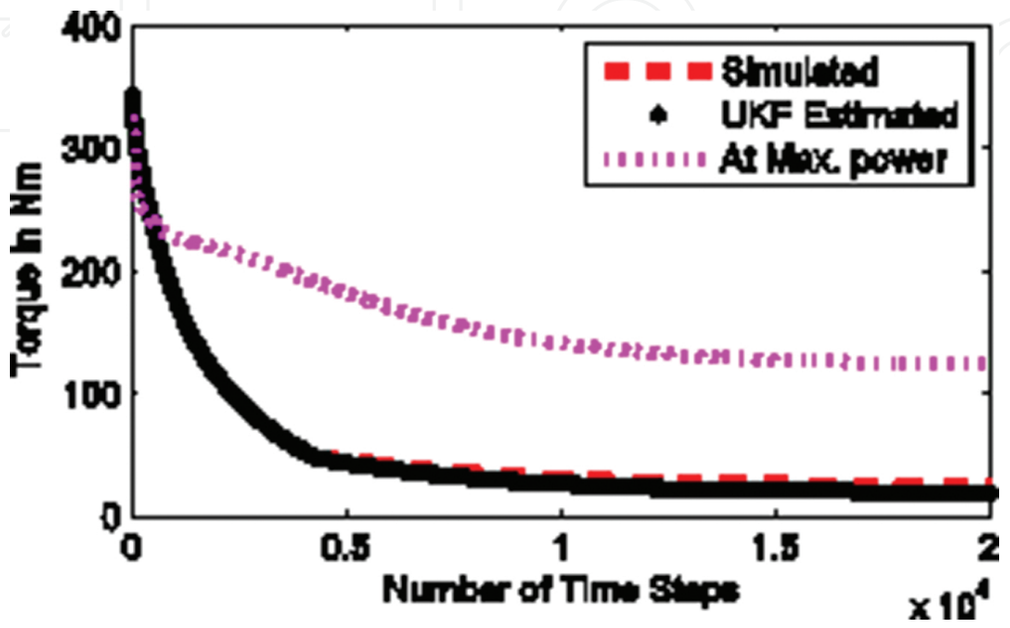

Figure 6. Turbine torque over the first 20,000 time steps and compared with the torque at the maximum available wind power.

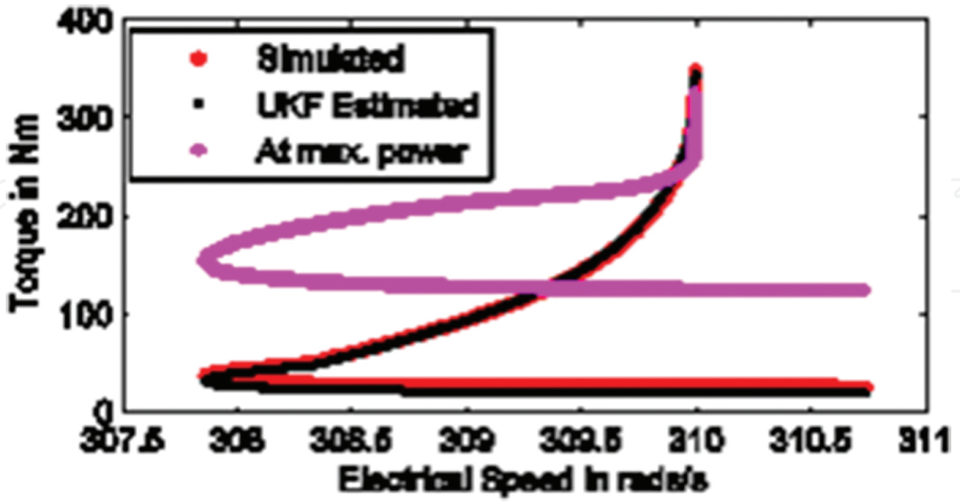

Figure 7. Turbine torque characteristic over the operating speeds in rad/s.

Figure 8 shows the growth of the estimated blade pitch angle and compared with the simulated blade pitch angle.

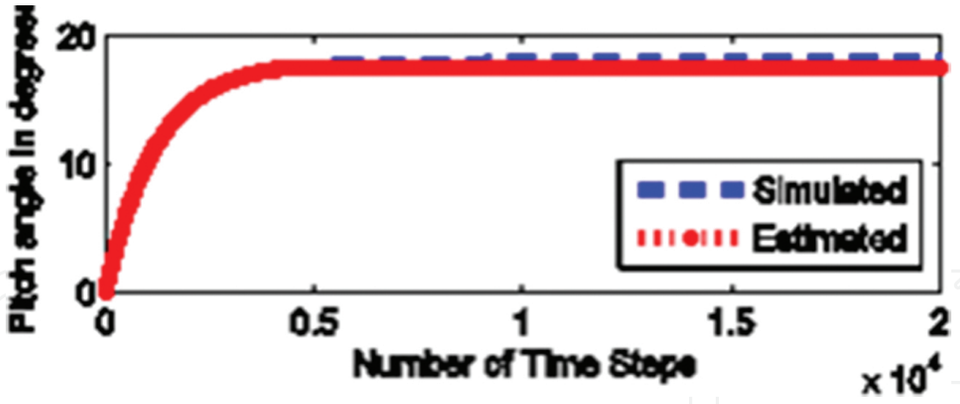

Figure 8. Estimated and simulated blade pitch angles compared.

6. Discussion and conclusions

In this chapter, a nonlinear UKF is used to provide the rotor-side control inputs and also in a tracking controller that ensures that the desired maximum power operating point is exactly tracked. As in ref. [3], the uncontrolled DFIG is unstable. Thus this necessitates the use of a stabilizing controller prior to implementing a MPPT filter. The MPPT filter tracks the maximum power point as the power is transferred from the wind to the turbine. The rotor-side control laws are synthesized by employing a H_2 optimal control law as described in ref. [3]. The MPPT filter is proposed and validated using non-linear UKF and EKF based estimation techniques. Thus an estimate of the actual power transferred from the turbine to the generator is maximized. It is shown that the MPPT filter can operate alongside the controller for regulating the blade pitch angle. The state estimation method is based on the UKF which is compared with the traditional EKF and is shown to be superior. The validation of the algorithm is carried out by simulating real wind velocity profiles from a white noise generator and using low order spectrum shaping filters that are derived from approximations of the Kaimal wind velocity spectrum. The MPPT algorithm is successfully demonstrated in the case significant levels of wind disturbances present and with the independently controlled variable pitch blades.

The advantages of using stochastic optimal control theory and nonlinear optimal control are discussed in ref. [3]. In this chapter it has been demonstrated that the MPPT control filter which acts as an outer-loop controller, continuously seeks to maximize the power absorbed by the wind turbine while the inner loop estimator continuously estimates and updates the states including the blade pitch angle (which was held fixed in ref. [3]). The MPPT control filter included a feedback signal estimated using the Newton-Raphson formula at each time step, just as in ref. [3]. One can estimate the wind power captured by the turbine and it indicates that the filter is seeking to operate within 5–9% of the simulated operating maximum power point by controlling the speed of the rotor after a 0.5 s delay, which allows the UKF to estimate the states and the unknown blade pitch angle without a significant error and to eliminate the

influence of power transients. The maximum available power in the wind is computed, as in ref. [3], by assuming that the wind is frozen at its maximum magnitude before it encounters the blades and the deterministic formula for the maximum power coefficient $C_p(\lambda)_{\max}$, is used to calculate it. In steady state the estimated maximum turbine power was generally uniformly less than the maximum available power, the difference being accounted for by the losses due to the finite and variable blade pitch angle, and the losses due to viscous frictional torques.

Finally the MPPT algorithm, based on the nonlinear state estimation using the UKF, is shown to perform, even when the blade pitch angles are dynamically varied and the introduction of the blade dynamics does not cause any additional instabilities when compared with the case of fixed blades considered in ref. [3]. The maximum power transfer achieved is less than in ref. [3], unless the blade is assumed to be fixed with the pitch angle set at zero.

Author details

Ranjan Vepa

Address all correspondence to: r.vepa@qmul.ac.uk

School of Engineering and Material Science, Queen Mary University of London, London

References

[1] Burton T, Sharpe D, Jenkins N, Bossanyi E. Wind Energy Handbook. John Wiley & Sons Ltd, England, 2001.

[2] Connor B, Leithead WE. Investigation of fundamental trade-off in tracking the Cpmax curve of a variable speed wind turbine. In: Proceedings of the 12th British Wind Energy Conference, 1993. pp. 313–317.

[3] Vepa R. Nonlinear, optimal control of a wind turbine generator. IEEE Transactions on Energy Conversion, 2011; 26(2):468–478.

[4] Fan L, Yin H, Miao, Z. On active/reactive power modulation of DFIG-based wind generation for inter-area oscillation damping. IEEE Transactions on Energy Conversion, 2011; 26(2):513–521.

[5] Shree KHP, Ram Kumar SVJ. Decoupled control of active and reactive powers of DFIG with cascaded SPWM converters. International Journal of Engineering Science and Technology, 2011; 3(10):7540–7545.

[6] Dendouga A, Abdessemed R, Bendaas ML, Chaiba A. Decoupled active and reactive power control of a doubly fed induction generator (DFIG). In: Proceedings of the 15th

Mediterranean Conf. on Control and Automation, Athens, Greece, July 27–29, 2007, Paper No. T26-004.

[7] Peresada S, Tilli A, Tonielli A. Power control of a doubly fed induction machine via output feedback. Control Engineering Practice, 2004; 12:41–57.

[8] Rosas P. Dynamic influences of wind power on the power system (PhD Thesis). Technical University of Denmark: Ørsted Institute, Section of Electric Power Engineering, March 2003.

[9] Slootweg JG, de Haan SWH, Polinder H, Kling WL. General model for representing variable speed wind turbines in power systems dynamics simulations. IEEE Transactions on Power Systems, 2003; 18(1):144–151.

[10] Padfield GD. Helicopter Flight Dynamics, Blackwell Science Ltd, Oxford, 1996.

[11] Fox ME. Blade mounted actuation for helicopter rotor control (MSc thesis). Boston: Massachusetts Institute of Technology, June 1993. pp. 83–125.

[12] Pitts DM, Peters DA. Theoretical predictions of dynamic-inflow derivatives. Vertica, 1981; 5:21–34.

[13] Tangler JL, Kocurek JD. Wind turbine post-stall airfoil performance characteristics guidelines for blade-element momentum methods. In: Proceedings of the 43rd AIAA Aerospace Sciences Meeting and Exhibit, Reno, Nevada, January 10–13, 2005, NREL/CP-500-36900.

[14] Tangler JL, Ostowari C. Horizontal axis wind turbine post stall airfoil characteristics synthesization. In: DOE/NASA Wind Turbine Technology Workshop, Cleveland, Ohio, May 1984, SERI/TP-257-4400, UC Category 261, DE91002198.

[15] Viterna LA, Corrigan RD. Fixed pitch rotor performance of large horizontal axis wind turbines. In: DOE/NASA Workshop on Large Horizontal Axis Wind Turbines, Cleveland, Ohio, July 1981.

[16] Vepa R. Wind power generation and control. In: Dynamic Modelling Simulation and Control of Energy Generation, Lecture Notes in Energy Series No. 20, Springer Verlag, London, 2013, Chapter 4.

[17] Julier SJ, Uhlmann J, Durrant-Whyte HF. A new method for the nonlinear transformation of means and covariances in filters and estimators. IEEE Transactions on Automatic Control, 2000; 45(3):477–482.

[18] Julier SJ and Uhlmann JK. Unscented filtering and nonlinear estimation. Proceedings of the IEEE, 2002; 92:401–422.

[19] Julier SJ. The scaled unscented transformation. In: Proceedings of the American Control Conference, 2002; 6:4555–4559.

[20] Pan S, Su H, Wang H, Chu J. The study of joint input and state estimation with Kalman filtering. Transactions of the Institute of Measurement and Control, 2011;33(8):901–918; doi:10.1177/0142331210361551.

[21] Hohm DP, Ropp ME. Comparative study of maximum power point tracking algorithms. Progress in Photovoltics: Research and Applications, 2003; 11(1):47–62.

[22] Yu GJ, Jung YS, Choi JY, Kim GS. A novel two-mode MPPT control algorithm based on comparative study of existing algorithms. Solar Energy, 2003;76:455–463.

[23] Bhowmik S, Spee R, Enslin JHR. Performance optimization for doubly fed wind power generation systems. IEEE Transactions on Industry Applications, 1999; 35(4):949–958.

[24] Qiao W, Gong X, Qu L. Output maximization control for DFIG wind turbines without using wind and shaft speed measurements. In: IEEE Energy Conversion Congress and Exposition, 2009, ECCE 2009. DOI: 10.1109/ECCE.2009.531613, pp. 404–410.

[25] Koutroulis E, Kalaitzakis K. Design of a maximum power tracking system for wind-energy-conversion applications. IEEE Transactions on Industrial Electronics, 2006; 53(2):486–494.

[26] Kawabe I, Morimoto S, Sanada M. Output maximization control of wind generation system applying square-wave operation and sensorless control. In: Power Conversion Conference, Nagoya, Japan, April 2007; 1:203–209.

[27] Munteanu I, Iuliana-Bratcu A, Cutululis N-A, Ceanga, E. Optimal control of wind energy systems: towards a global approach. Advances in Industrial Control, Springer, 1st Edition, 2008; 5:109–128.

[28] Abo-Khalil AG, Lee D-C. MPPT control of wind generation systems based on estimated wind speed using SVR. IEEE Transactions on Industrial Electronics, 2008; 55(3):1489–1490.

[29] Boukhezzar B, Siguerdidjane H. Nonlinear control of variable speed wind turbines without wind speed measurement. In: Proceedings of the 44th IEEE Conference on Decision and Control, Seville, Spain, December 12–15, 2005, pp. 3456–3461.

IntechOpen